Influence of deposition pressure on the structural, optical and electrical properties of Sb_2Se_3 thin films grown by RF magnetron sputtering

FEI ZHAO[a], JIAHUA TAO[a], YIXIN GUO[a], CHUANHE MA[a], JINCHUN JIANG[a,b,*], JUNHAO CHU[a,b,c]
[a]*Key Laboratory of Polar Materials and Devices, Ministry of Education, Department of Electronic Engineering, East China Normal University, Shanghai 200241, China*
[b]*Shanghai Center for Photovoltaics, Shanghai 201201, China*
[c]*Shanghai Institute of Technical Physics, Chinese Academy of Sciences, Shanghai 200083, China*

In this paper, Sb_2Se_3 thin films were deposited on quartz substrates by radio frequency (RF) magnetron sputtering at different deposition pressures. The structural, optical and electrical properties of the Sb_2Se_3 films were investigated by XRD, Raman, XPS, SEM, Hall Effect and UV-Vis measurements. With optimized deposition pressure of 0.5 Pa, the fabricated Sb_2Se_3 film has the highest crystallinity, the most stable valence of Se^{2-} and Sb^{3+}, the maximum mobility (21.54 $cm^2 V^{-1} s^{-1}$) and the suitable optical band gap (1.33 eV). This study provides a guideline to prepare Sb_2Se_3 film for photovoltaics.

(Received July 27, 2018; accepted June 14, 2019)

Keywords: Sb_2Se_3 thin films, Magnetron sputtering, Crystallinity, Electrical mobility, Optical band gap

1. Introduction

The crisis of energy needs is the major concern in the world nowadays, which make it significant to develop sustainable energy involving solar energy. Solar cell is one of the most attractive technology for solar energy conversion and storage, which has been investigated for many decades. Among various kinds of solar cells, the film solar cell with the high efficiency and stability is promising for large-scale commercial application [1]. Antimony triselenide (Sb_2Se_3), a nontoxic and earth abundant constituent, has been attracted much attention as an absorber in solar cell application [2]. Sb_2Se_3 material possesses excellent optoelectronic properties such as suitable band gap of 1.0–1.3 eV, decent carrier mobility, long carrier lifetime, high absorption coefficient (>10^5 cm^{-1}) in the visible range and benign grain boundaries [3-5]. These characteristics further reinforce its rivalrousness as a new non-toxic absorber material for photovoltaics. During the past decades, several methods have been applied to prepare Sb_2Se_3 films, such as chemical bath deposition [6] and electrodeposition [7-8]. The main flaw is time-consuming and more importantly, the unavoidable incorporation of impurities attributed to solvent or oxides. Recently, Chen C. [9] reported an amusing method for fabricating Sb_2Se_3 films via evaporating an excess of Sb_2Se_3 powder with a high temperature. High photoelectric of the gained thin films has been reported. Up to now, there is no attention on the influence of deposition pressure on the structural, optical and electrical characteristics of Sb_2Se_3 thin films grown by magnetron sputtering method. This technology has however some merits including good film-to-substrate adhesion, low cost, good uniformity and low operating temperature [10-12].

In this work, we report an effective sputtering way of growing well-crystallized, compact and uniform Sb_2Se_3 thin films at suitable depositing pressure. This technique can reduce the introduction possibility of impurity which is intrinsic to the non-vacuum environment and prevent excess consumption of Sb_2Se_3 in the thermal evaporation process. The effectiveness, as well as the merits, of the Sb_2Se_3 films deposited at various pressure were investigated systematically by analyzing the structure and optical–electrical characteristics of the films.

2. Experimental details

Sb_2Se_3 films were deposited on 20×20×1.1 mm^3 quartz substrates via radio frequency (RF) magnetron sputtering of a 99.999% pure Sb_2Se_3 target. Prior to deposition, the quartz substrates were ultrasonically cleaned in acetone, alcohol and deionized water for 15 min separately. Afterwards, they were blow-dried with nitrogen gas and placed into the sputtering chamber. The distance between the target and the substrate was 6 cm and the substrate holder was whirled at 10 rpm with the purpose of depositing homogeneous film. The base pressure of vacuum chamber was approximately evacuated down to 6.0×10^{-4} Pa, and then the growth temperature was kept at 320 °C during the plasma process. During deposition, the RF power and sputtering time was fixed at 75 W and 40 min, respectively. High-purity (99.999%) Ar was introduced into the vacuum chamber with flow rates of 40 sccm, and the deposition was carried out at working pressure of 0.2 Pa, 0.4 Pa, 0.5 Pa, 0.6 Pa and 0.8 Pa, respectively. At the beginning of each sputtering process, the Sb_2Se_3 target surface was presputtered for about 10 min to remove the surface contaminants.

Crystal structures of the films were examined by X-ray diffraction (XRD, Rigku D/max 2550 V) in a 2θ range of 10°-70°. Morphologies of the films were observed via scanning electron microscopy (SEM, JEOL) with an acceleration voltage of 10 kV. The chemical valence was obtained via using X-ray photoelectron spectroscopy (XPS, ESCALAB 250Xi) with a monochromatic Al Ka X-ray source of 1486.6 eV, and Raman spectra were measured using a He–Cd laser with an excitation wavelength of 532 nm by a Confocal Laser Spectrometer (LabRAM HR 800 UV). The transmittance spectra were characterized by using a UV-VIS spectrophotometer (Cary5000) in the wavelength scope of 300-1800 nm. The electrical properties of the films were studied by Hall-effect Measurement System (Ecopia, HMS3000) using Van der Pauw technique at room temperature.

3. Results and discussion

3.1. Structural properties

Fig. 1 shows the XRD spectra of Sb_2Se_3 thin films at different deposition pressures. It can be seen from Fig. 1 that multiple diffraction peaks are observed, and the positions of all these diffraction peaks are in good agreement with the standard diffraction mode of orthorhombic Sb_2Se_3 (JCPDS Card No. 15-0861), confirming their polycrystalline nature. Simultaneously, a strong diffraction peak corresponding to the (002) plane can be observed for all Sb_2Se_3 films, indicating that the Sb_2Se_3 films grew towards (002) preferred orientation. When the deposition pressure is increased from 0.2 Pa to 0.5 Pa, the diffraction peak intensity continuously increases, indicating that the grain density of the film is heightened. However, as the deposition pressure increases to 0.8 Pa, the intensity of the diffraction peak appears a slowly decreasing trend, revealing that the grain density of the film decreases. The above results show that its diffraction peak is the strongest at the working pressure of 0.5 Pa, which indicates that the film has an optimal crystallinity.

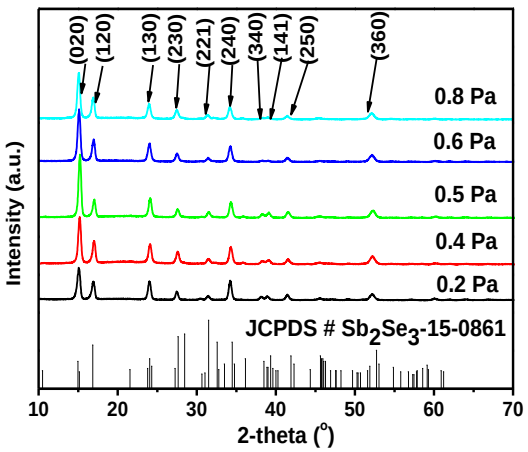

Fig. 1. XRD spectra of Sb_2Se_3 thin films under different deposition pressures

Raman spectroscopy was utilized as an extra method to analyse the phase purity and crystallinity of Sb_2Se_3 thin films. Fig. 2 shows the Raman spectra of Sb_2Se_3 thin films prepared at various deposition pressures. Results reveal some characteristic patterns are consistent with the reported ones [13], i.e., marked as M1 (153.3 cm^{-1}), M2 (190.4 cm^{-1}), and M3 (210.8 cm^{-1}), demonstrating the presence of the pure Sb_2Se_3 phase. The foremost M2 mode frequency is at 190.4 cm^{-1}, which is attributed to the heteropolar vibrations of Sb-Se bond [14]. The intensity of Sb_2Se_3 peaks increases with the deposition pressure varying from 0.2 to 0.5 Pa, which indicates that the crystallinity of the Sb_2Se_3 films is continuously improved. However, the peak intensity continues to decrease when the pressure increases to 0.8 Pa, indicating that the crystallinity of the film is deteriorated. The most intense peak at 190.4 cm^{-1} was obtained with the Sb_2Se_3 films deposited at pressure of 0.5 Pa. This demonstrated a well-crystallized thin film, which is in accordance with the XRD result.

The above phenomenon can be explained by the fact that at a relatively lower pressure of 0.2-0.5 Pa, the clusters of atoms sputtered from the target possess low feasibility of colliding with argon ions on their way to the quartz substrate and their kinetic energy and mobility are maintained at high levels. Meanwhile, more and more atomic groups fly to the surface of the substrate with the increasing pressure, which are contributed to promote the growth of crystalline grains. However, at higher pressure of 0.6-0.8 Pa, the sputtering atomic clusters have more opportunities to collide with argon ions, which decreases the number, kinetic energy and mobility of the atomic clusters arriving at the substrate. Thence, these factors above restrain the growth of crystal.

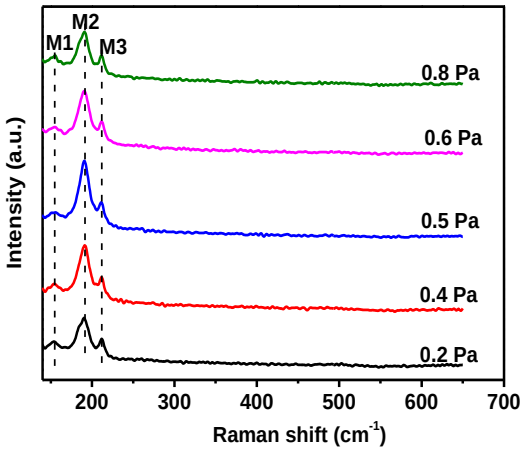

Fig. 2. Raman spectra of Sb_2Se_3 films with different deposition pressures

Surface morphology of the Sb_2Se_3 film deposited at a pressure of 0.5 Pa is shown in Fig. 3. It can be observed that the surface of the Sb_2Se_3 film is flat and the crystalline grains are compact, indicating that the Sb_2Se_3 film prepared under this experimental condition has high

crystallinity. This is in good agreement with the analysis of XRD and Raman. In addition, benign grain boundaries are clearly found from the partially enlarged image (the inset) of the film. There are however some small dots on the surface of the film, which is attributed to the gold particles. This is due to the fact that a layer of gold film was sprayed on the Sb_2Se_3 film surface in order to enhance the conductivity of the film so that the surface morphology of the film could be more clearly observed.

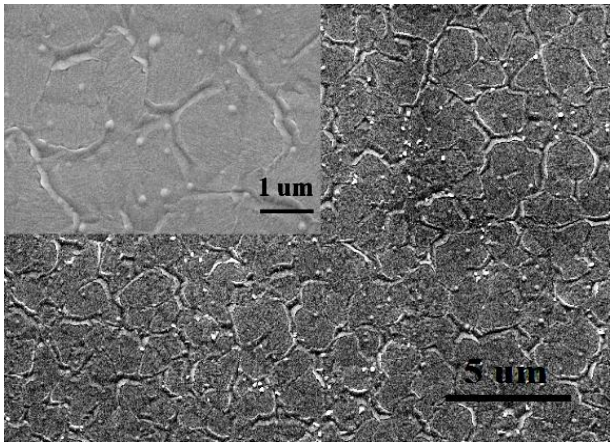

Fig. 3. Surface SEM image and the partially enlarged image (the inset) of Sb_2Se_3 film deposited at a pressure of 0.5 Pa

To investigate the constituent element valence states of the Sb_2Se_3 films, XPS examination was conducted. Fig. 4 shows the binding energies (BE) gained from the high resolution core level spectra areas of Sb3d and Se3d. Apart from the charge compensation via the flood gun related with the spectrometer, the BE of all peaks was revised employing C1s energy at 284.6 eV. The spin–orbit-coupled doublet of Sb3d core levels is divided into $3d_{5/2}$ (528.53 eV) and $3d_{3/2}$ (538.11 eV) with the separation of 3d doublet via 9.58 eV ascribed to the charge state of Sb^{3+}. The Se3d core levels of $3d_{5/2}$ and $3d_{3/2}$ emerges at 52.78 and 53.68 eV with a doublet separation of 0.90 eV, in consonance with the Se in metal selenide [15]. The prospective valence state of Sb^{3+} and Se^{2-} in all Sb_2Se_3 samples reveals the purity of the Sb_2Se_3 phase. The peak intensity of $Sb3d_{5/2}$, $Sb3d_{3/2}$, $Se3d_{5/2}$, and $Se3d_{5/2}$ increases when the deposition pressure increases from 0.2 Pa to 0.5 Pa, which indicates that the valence stability of the element enhanced in the Sb_2Se_3 film. However, their peaks intensity weakens as the pressure further increases to 0.8 Pa, which reveals the decline of valence stability in the Sb_2Se_3 film. The above results show that the peak intensity is the highest at the deposition pressure of 0.5 Pa, demonstrating that the most stable valence state was clearly observed in the Sb_2Se_3 film prepared under this experimental condition.

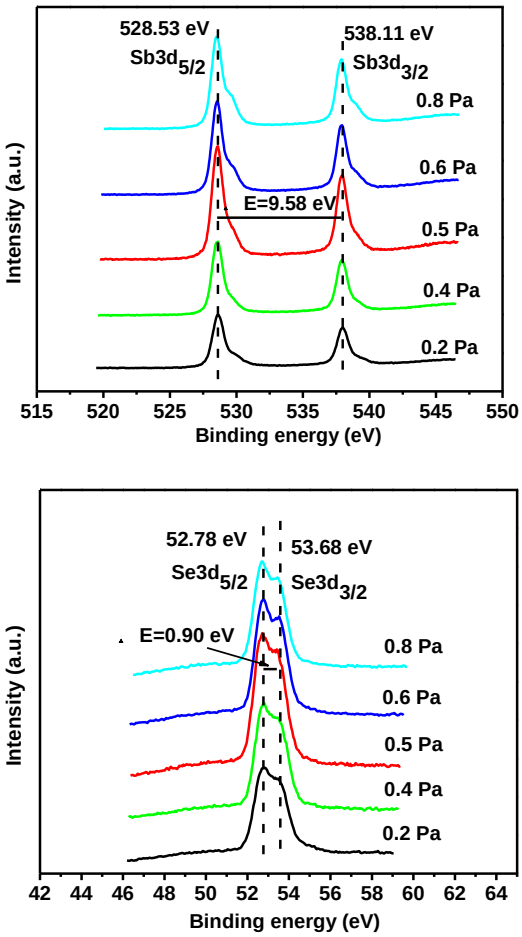

Fig. 4. XPS spectra of Sb_2Se_3 films with the deposition pressures of 0.2, 0.4, 0.5, 0.6 and 0.8 Pa

The Se/Sb ratio of Sb_2Se_3 films deposited at different pressure is given in Table 1. It can be seen that the Se/Sb ratio decreases by increasing Ar gas pressure. This may be due to the fact that more and more argon ions bombard the surface of the target and generate a large amount of selenium and antimony atoms with the increasing gas pressure. Meanwhile, since the atomic mass of selenium is less than that of antimony, the number of collision between selenium atoms and argon ions is greater than the collision number of antimony atoms with argon ions, leading to the reduction of selenium content in the Sb_2Se_3 films.

Table 1. Composition of Sb_2Se_3 films deposited at different pressures

pressure (Pa)	Sb(at%)	Se(at%)	Se/Sb
0.2	41.69	58.31	1.40
0.4	42.18	57.82	1.37
0.5	42.70	57.30	1.34
0.6	43.69	56.31	1.29
0.8	45.16	54.84	1.21

3.2. Optical and electrical properties

Fig. 5a shows the transmittance spectra of the Sb_2Se_3 films deposited at different pressures. The absorption edge of the film gradually shifts toward the short wavelength in the range of 800-925 nm by increasing deposition pressure, denoting that the optical band gap of the Sb_2Se_3 film narrows with increasing the deposition pressure. In the light of the Tauc's method [16], the band gaps of Sb_2Se_3 films at different pressures could be calculated via utilizing the following formula,

$$(ahv)^2 = B(hv - Eg)$$

where α represents the absorption coefficient, hν represents the photon energy, B represents a constant associated with effective mass, respectively. By fitting $(\alpha h\nu)^2$ versus hν curves linearly, the band gap could be obtained from the transverse axis intercept for Sb_2Se_3 film transmittance detected between 0.2 Pa and 0.8 Pa (Fig. 5b). It can be observed that the band gap increases from 1.29e to 1.35eV when the pressure increases from 0.2 Pa to 0.8 Pa, which reveals a good consistency with the previous analysis. This band gap behavior is originated from the reduction in Se content in the Sb_2Se_3 films, which is caused by the more intense collision of selenium atoms with Ar ions during the sputtering process.

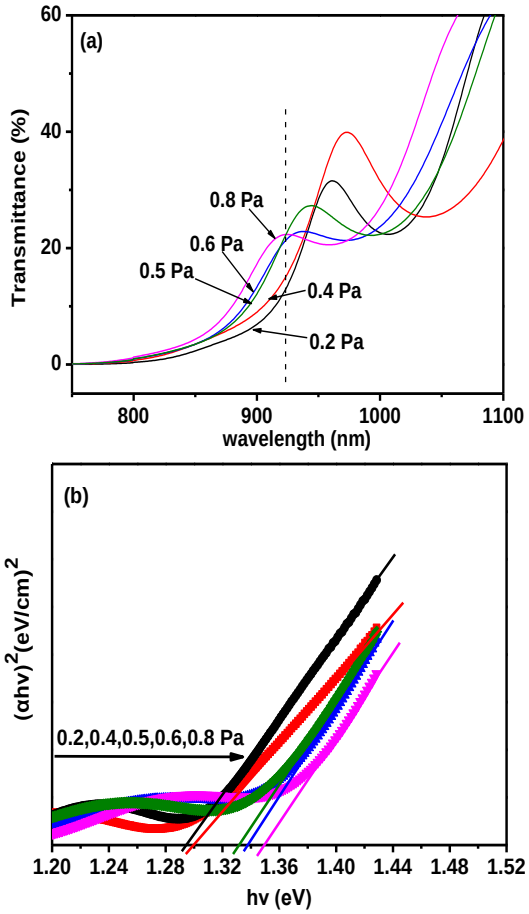

Fig. 5. (a) Transmission spectra of Sb_2Se_3 films and (b) graphs of $(\alpha h\upsilon)^2$ versus hυ for Sb_2Se_3 films with various deposition pressures

The electrical properties of pure Sb_2Se_3 films were determined by Hall effect measurement system adopting Van der Pauw technique at room temperature. As depicted in Fig. 6, all films are p-type semiconductors. Carrier concentrations are 5.10×10^{13}, 2.93×10^{13}, 2.37×10^{13}, 1.48×10^{13} and 1.35×10^{13} cm^{-3}, respectively, with increasing deposition pressure. For mobility results, it increases from 9.24 to 21.54 $cm^2\ V^{-1}\ s^{-1}$ as deposition pressure increases from 0.2 to 0.5 Pa but slightly degrades to 19.47 $cm^2\ V^{-1}\ s^{-1}$ at 0.8 Pa. For resistivity, sample deposited at low pressure 0.2 Pa is 31,420 Ω • cm but it decreases to 15,920, 10,387, 14,076 and 19,529 Ω • cm with increasing deposition pressure. Since the mobility is near 10 $cm^2\ V^{-1}\ s^{-1}$ for Cu_2ZnSnS_4 film, Sb_2Se_3 film with mobility approximately 22 $cm^2\ V^{-1}\ s^{-1}$ shows a good electrical property for film solar cells [17]. Compared with the reported properties in electricity, our experimental data reveal promising prospects and the significance of process control.

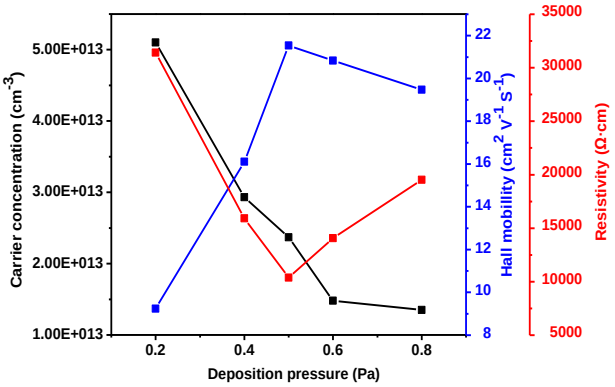

Fig. 6. The electrical properties of Sb_2Se_3 films with different deposition pressures

4. Conclusion

In this paper, Sb_2Se_3 thin films were successfully fabricated on the quartz substrate by employing RF magnetron sputtering method at different Ar gas pressures. The effects of deposition pressure on the structural, optical and electrical properties of Sb_2Se_3 thin films were investigated systematically. XRD, SEM and Raman results indicates that when the deposition pressure increases from 0.2 Pa to 0.8 Pa, the crystallinity of the polycrystalline Sb_2Se_3 films increases first and then decreases. It is determined by XPS results that the valence stability of Se^{2-} and Sb^{3+} enhances first and then weakens by increasing Ar gas pressure. Hall measurement manifests that as the deposition pressure increases from 0.2 Pa to 0.5 Pa, the electrical mobility increases from 9.24 $cm^2\ V^{-1}\ s^{-1}$ to 21.54 $cm^2\ V^{-1}\ s^{-1}$. However, the mobility decreases to 19.47 $cm^2\ V^{-1}\ s^{-1}$ with the deposition pressure of 0.8 Pa. In addition, the optical band gap values are 1.29, 1.30, 1.33, 1.34 and 1.35 eV for the samples of 0.2, 0.4, 0.5, 0.6 and 0.8 Pa, respectively. Therefore, the crystallinity, valence stability, electrical mobility, and optical band gap of the film could

be improved by adjusting the Ar gas pressure. The prepared Sb_2Se_3 film has the highest crystallinity, most stable valence of the elements, maximum mobility (21.54 $cm^2\ V^{-1}\ s^{-1}$) and suitable optical band gap at the Ar gas pressure of 0.5 Pa. It is expected to prepare high-quality Sb_2Se_3 films by optimizing the sputtering process, and apply them to the field of solar cells.

Acknowledgements

This work was financed by the National Science Foundation of China (Grant No. 61704057), and Major State Basic Research Development Program of China (Grant No. 2013CB922300).

References

[1] C. Yuan, X. Jin, G Jiang, W. Liu, C. Zhu, J. Mater. Sci. Mater. Electron. **27**, 8906 (2016).
[2] Y. Yu, R. H. Wang, Q. Chen, L. M. Peng, J. Phys. Chem. B **110**, 13415 (2006).
[3] J. Yang, Y. Q. Lai, Y. Y. Fan, Y. Jiang, D. Tang, L. X. Jiang, F. Y. Liu, J. Li, RSC Adv. **5**, 85592 (2015).
[4] L. Wang, D. B. Li, K. Li, C. Chen, H. X. Deng, L. Gao, Y. Zhao, F. Jiang, L. Y. Li, F. Huang, Y. S. He, H. S. Song, G D. Niu, J. Tang, Nat. Energy **2**, 17046 (2017).
[5] Y. Zhou, L. Wang, S. Y. Chen, S. K. Qin, X. S. Liu, J. Chen, D. J. Xue, M. Luo, Y. Z. Cao, Y. B. Chen, E. H. Sargent, J. Tang, Nat. Photon. **9**, 409 (2015).
[6] M. R. Filip, C. E. Patrick, F. Giustino, Phys. Rev. B **87**, 2450 (2013).
[7] J. Y. Li, B. Wang, F. Y. Liu, J. Liu, M. Jia, Y. Q. Lai, J. Li, Y. X. Liu, ECS Solid State Lett. **1**, Q29 (2012).
[8] T. T. Ngo, S. Chavhan, I. Kosta, O. Miquel, H. J. Grande, R. Tena-Zaera, ACS Appl. Mater. Interfaces **6**, 2836 (2014).
[9] C. Chen, W. Li, Y. Zhou, M. Luo, X. S. Liu, K. Zeng, B. Yang, C. W. Zhang, J. B. Han, J. Tang, Appl. Phys. Lett. **107**, 1301846 (2015).
[10] P. Sharma, K. Sreenivas, K. V. Rao, J. Appl. Phys. **93**, 3963 (2003).
[11] H. K. Dong, N. G Cho, K. S. Kim, S. Han, H. G Kim, J. Electroceram. **22**, 82 (2009).
[12] G X. Liang, X. H. Zhang, H. L. Ma, J. G Hu, B. Fan, Z. K. Luo, Z. H. Zheng, J. T. Luo, P. Fan, Sol. Energy Mater. Sol. Cells **160**, 257 (2017).
[13] P. P. Kong, F. Sun, L. Y. Xing, J. Zhu, S. J. Zhang, W. M. Li, Q. Q. Liu, X. C. Wang, H. K. Moo, C. Q. Jin, Sci. Rep. **4**, 66879 (2014).
[14] X. C. Ma, Z. D. Zhang, X. Wang, S. T. Wang, F. Xu, Y. T. Qian, J. Cryst. Growth **263**, 491 (2004).
[15] R. C. Jin, Z. Q. Liu, L. X. Yang, J. S. Liu, Y. B. Xu, G. H. Li, J. Alloy. Compd. **579**, 209 (2013).
[16] G X. Liang, Z. H. Zheng, P. Fan, J. T. Luo, J. G Hu, X. H. Zhang, H. L. Ma, B. Fan, Z. K. Luo, D. P. Zhang, Sol. Energy Mater. Sol. Cells **174**, 263 (2017).
[17] C. Yuan, L. Zhang, W. Liu, C. Zhu, Sol. Energy **137**, 256 (2016).

*Corresponding author: jcjiang@ee.ecnu.edu.cn